Water **2014**, *6*, 1785-1806; doi:10.3390/w6061785

OPEN ACCESS

water

ISSN 2073-4441

www.mdpi.com/journal/water

Article

Photocatalytic Degradation of Phenol and Phenol Derivatives Using a Nano-TiO_2 Catalyst: Integrating Quantitative and Qualitative Factors Using Response Surface Methodology

Marissa Choquette-Labbé, Wudneh A. Shewa, Jerald A. Lalman * and Saravanan R. Shanmugam

Department of Civil and Environmental Engineering, University of Windsor, 401 Sunset Ave., Windsor, ON N9B 3P4, Canada; E-Mails: marissajustine@hotmail.com (M.C.-L.); shewa@uwingmail.uwindsor.ca (W.A.S.); ramiah@uwingmail.uwindsor.ca (S.R.S.)

* Author to whom correspondence should be addressed; E-Mail: lalman@uwindsor.ca; Tel.: +1-519-253-3000 (ext. 2519); Fax: +1-519-971-3686.

Received: 23 April 2014; in revised form: 27 May 2014 / Accepted: 5 June 2014 / Published: 17 June 2014

Abstract: Due to the toxicity effects and endocrine disrupting properties of phenolic compounds, their removal from water and wastewater has gained widespread global attention. In this study, the photocatalytic degradation of phenolic compounds in the presence of titanium dioxide (TiO_2) nano-particles and UV light was investigated. A full factorial design consisting of three factors at three levels was used to examine the effect of particle size, temperature and reactant type on the apparent degradation rate constant. The individual effect of TiO_2 particle size (5, 10 and 32 nm), temperature (23, 30 and 37 °C) and reactant type (phenol, o-cresol and m-cresol) on the apparent degradation rate constant was determined. A regression model was developed to relate the apparent degradation constant to the various factors. The largest photocatalytic activity was observed at an optimum TiO_2 particle size of 10 nm for all reactants. The apparent degradation rate constant trend was as follows: o-cresol > m-cresol > phenol. The ANOVA data indicated no significant interaction between the experimental factors. The lowest activation energy was observed for o-cresol degradation using 5-nm TiO_2 particles. A maximum degradation rate constant of 0.0138 min^{-1} was recorded for o-cresol at 37 °C and a TiO_2 particle size of 13 nm at a D-optimality value of approximately 0.98. The response model adequately related the apparent degradation rate constant to the factors within the range of factors under consideration.

Keywords: photocatalysis; titanium dioxide; o-cresol; m-cresol; phenol; statistical modeling; quantitative factors; qualitative factors

1. Introduction

Phenols, also termed total phenols or phenolics, are important due to their widespread use in many manufacturing processes. However, these chemicals pose a serious threat to many ecosystems, water supplies and human health because of their inertness, toxicity, endocrine disrupting abilities and carcinogenic behavior [1,2]. The United States, Canada and the European Union have included some phenols in their list of priority pollutants [3–5]. Phenol is commonly employed in the manufacturing of phenolic resins, bisphenol A, caprolactam and chlorophenols such as pentachlorophenol [1]. Cresols are isomeric mono-substituted phenols. Commercially, cresol is produced as a by-product from the fractional distillation of crude oil and coal tars and the gasification of coal. Phenol and its derivatives have been identified in effluents from petroleum refining [6] pulp and paper manufacturing [7], coal processing [8] and chemical production facilities [9]. Oil-shale processing is another industry that produces effluents containing phenol and cresols [10].

Removing phenolic compounds from wastewaters and drinking water supplies has received widespread attention recently because of their toxic and endocrine disrupting properties [11]. Phenols can be removed by physical processes such as flocculation, precipitation, granular activated carbon (GAC) or reverse osmosis (RO) [12]. Enzymes and microorganisms have also been employed to remove phenols. Studies by Cooper and Nicell [13] have shown over 97% phenol removal using an enzymatic process. However, using enzymes is impractical because of high catalyst cost and short-lived catalytic activity [13]. Biological processes have also been used to remove phenolic compounds. However, in many cases, phenols are inhibitory to microorganisms at threshold levels [14,15].

Inadequate removal of phenolic compounds by conventional biological treatment methods has forced researchers to develop alternative treatment approaches. Advanced oxidative processes (AOP) are successful in removing complex organic contaminants because they can achieve complete oxidation [16]. AOP offer a distinct advantage over many conventional treatment methods, such as biological processes, because faster degradation rates are accomplished and contaminants are degraded rather than transferred from one phase to another. In addition, there is no requirement for by-product disposal [17]. AOP processes can be configured using a combination of chemical and physical agents such as a combination of oxidizing agents, an oxidizing agent plus ultraviolet, catalyst or ultrasound and a catalyst plus ultraviolet [18]. In all AOP processes, the degradation of organics is mediated by the generation of •OH radicals [19]. Recent overwhelming research interest in using TiO_2 as a photocatalyst is attributed to its excellent abilities in completely degrading a wide array of organic compounds to CO_2 plus H_2O [15,20,21]. Hence, in the present work, TiO_2 was selected to examine the degradation of several phenolic compounds. Titanium dioxide exists primarily as anatase, rutile and brookite. In comparison to rutile and brookite, the anatase phase is catalytically more active [22,23]. Factors such as the type of photocatalyst and the composition, light intensity, initial substrate concentration, amount of catalyst, particle size, pH of the reaction medium, ionic components in water, solvent types, oxidizing agents/electron acceptors, mode of catalyst application and calcinations temperature can affect the photocatalytic degradation of organic compounds [24]. The impact of various factors on photocatalytic reactions has been reported in many studies; however, few studies have examined the interaction effects of different variables on process performance. Studies assessing the impact of interaction factors on TiO_2 photocatalysis are limited [25,26] and in an effort to address this knowledge gap, this work will examine the effects of TiO_2 particle size, temperature and the chemical structure of similar structures (phenol and mono-substituted isomers (cresol isomers)) on the photocatalytic degradation rate.

Response surface methodology (RSM) is a collection of statistical techniques used to develop, improve and optimize processes. RSM tools are useful in predicting the effect of individual experimental factors, as well as locating interactions between the factors. RSM has been used extensively to assess the impact of quantitative variables on a response variable [27–29]; however, the use of this technique is limited, especially in cases involving quantitative, as well as qualitative variables [30,31]. The effect of single, squared and interaction terms on the response variable can be demonstrated using second order models. Examining the effects of quantitative, as well as qualitative variables on a response variable is routinely employed for analyzing data in disciplines such as science, social science and business [32,33]. Developing response models using qualitative and quantitative factors have been reported in several studies [34–36]; however, the technique has not been applied extensively in science and engineering applications.

One objective of this study was to develop a statistical model that relates the apparent degradation constant to TiO_2 catalyst particle size, temperature and reactant structure and subsequently, to assess the effects of the different factors on the apparent degradation rate constant. Another objective was to determine the optimum TiO_2 particle size for the maximum degradation of phenol and mono-substituted phenol isomers (o-cresol and m-cresol) with respect to the activation energy of the photocatalyst.

2. Materials and Methods

2.1. Phenols and Cresols

Phenol (99% purity) and m-cresol (99% purity) were procured from Sigma-Aldrich (Oakville, ON, Canada). o-Cresol (99% purity) was purchased from Anachemia Chemicals Ltd. (Toronto, ON, Canada). The chemicals were stored at 21 °C, and stock preparations were prepared on an as needed basis. The stock solutions were covered with Aluminum foil and refrigerated.

2.2. Titanium Dioxide

TiO_2 nanoparticles were procured from Alfa Aesar (Ward Hill, MA, USA). The characteristics for the three different TiO_2 anatase nanoparticles are shown in Table 1. Stock water suspensions of the TiO_2 nanoparticles (10,000 mg L^{-1}) were prepared and stored at 21 °C. The TiO_2 suspensions were pulse-sonicated at 20 kHz for 15 min using a VWR model 75HT sonicator (VWR, Mississauga, ON, Canada) to ensure homogeneous mixing prior to the reaction with the different reactants.

Table 1. The TiO_2 catalyst surface area.

Particle size (nm)	Surface area ($m^2\ g^{-1}$)
5 [1]	275 ± 15 [2]
10 [1]	131 ± 12 [2]
32 [1]	47 ± 2 [2]

Notes: [1] The particle size as per the manufacturer's specifications (Alfa Aesar, Ward Hill, MA, USA). [2] The surface area ($m^2\ g^{-1}$) of the TiO_2 nanoparticles was determined using a Brunauer–Emmett–Teller (BET) gas adsorption technique using a Quantachrome NOVA 1200e surface area analyzer (Quantachrome Instruments, Boynton Beach, FL, USA). The instrument temperature was set at 77 K, and nitrogen (BOC, Windsor, ON, Canada) was the adsorbate.

2.3. Experimental Design and Statistical Analysis

A three-factor, three-level full factorial design was conducted for a complete analysis of the different reaction conditions (Table 2). The change in structure between the different chemicals (phenol, o-cresol and m-cresol) was selected as the qualitative factor (z). The quantitative factors were temperature and particle size. The levels for temperature, a quantitative factor (x_1), were 23 °C, 30 °C and 37 °C, and the TiO_2 particle size levels (denoted as factor x_2) were 5 nm, 10 nm and 32 nm. The full experimental design is shown in Table 3. Statistical analysis of the data was conducted using Minitab 15 (Minitab Inc., State College, PA, USA) and Polymath 6.2 (Willimantic, CT, USA).

Table 2. Experimental design parameters.

Level	Factors					
	Reactant (R)	**(z)**	**Temperature (°C/K)**	**(x_1)**	**TiO_2 particle size (nm)**	**(x_2)**
	Type	Coded	Actual	Coded	Actual	Coded
1	phenol	−1	23/296	−1	5	−1
2	m-cresol	0	30/303	0	10	0
3	o-cresol	+1	37/313	+1	32	+1

Note: The assignment of coded variables to qualitative and quantitative parameters is based on Quinn and Keough [32].

Table 3. Photocatalytic reaction apparent degradation rate constants for different experimental conditions.

Expt #	Factors			Response				Residual
				Apparent Degradation rate constant [1] (min^{-1})				
	Temperature (°C)	TiO_2 diameter (nm)	Reactant	Experimental [2]		Predicted [2]		
				Average	SD	Average	SD	
1	23 ± 2	5	phenol	0.0069	0.0003	0.0073	0.0003	−0.0004
2	23 ± 2	5	m-cresol	0.0093	0.0003	0.0089	0.0002	0.0004
3	23 ± 2	5	o-cresol	0.0115	0.001	0.0106	0.0001	0.0009
4	30 ± 2	5	phenol	0.007	0.0002	0.0081	0.0003	−0.0011
5	30 ± 2	5	m-cresol	0.0093	0.0007	0.0098	0.0002	−0.0005
6	30 ± 2	5	o-cresol	0.0114	0.0017	0.0115	0.0001	−0.0001
7	37 ± 2	5	phenol	0.008	0.0002	0.0089	0.0003	−0.0009
8	37 ± 2	5	m-cresol	0.0116	0.0002	0.0106	0.0002	0.0010
9	37 ± 2	5	o-cresol	0.013	0.0003	0.0123	0.0001	0.0007

Table 3. *Cont.*

Expt #	Temperature (°C)	TiO_2 diameter (nm)	Reactant	Apparent degradation rate constant [1] (min^{-1}) Experimental [2] Average	SD	Predicted [2] Average	SD	Residual
10	23 ± 2	10	phenol	0.008	0.0001	0.0086	0.0002	−0.0006
11	23 ± 2	10	m-cresol	0.0098	0.0002	0.0103	0.0001	−0.0005
12	23 ± 2	10	o-cresol	0.0119	0.0003	0.0120	0.0000	−0.0001
13	30 ± 2	10	phenol	0.0101	0.0001	0.0094	0.0002	0.0007
14	30 ± 2	10	m-cresol	0.0115	0.0002	0.0111	0.0000	0.0004
15	30 ± 2	10	o-cresol	0.0119	0.0009	0.0128	−0.0001	−0.0009
16	37 ± 2	10	phenol	0.0117	0.0012	0.0103	0.0001	0.0014
17	37 ± 2	10	m-cresol	0.0123	0.0004	0.0119	0.0000	0.0004
18	37 ± 2	10	o-cresol	0.0128	0.0005	0.0136	−0.0001	−0.0008
19	23 ± 2	32	phenol	0.0023	0.0002	0.0020	0.0001	0.0004
20	23 ± 2	32	m-cresol	0.0042	0.0003	0.0036	0.0000	0.0006
21	23 ± 2	32	o-cresol	0.0052	0.0001	0.0053	−0.0001	−0.0001
22	30 ± 2	32	phenol	0.0028	0	0.0028	0.0001	0.0000
23	30 ± 2	32	m-cresol	0.0046	0.0003	0.0045	0.0000	0.0001
24	30 ± 2	32	o-cresol	0.0063	0.0001	0.0061	−0.0001	0.0002
25	37 ± 2	32	phenol	0.0034	0.0003	0.0036	0.0001	−0.0002
26	37 ± 2	32	m-cresol	0.005	0.0003	0.0053	0.0000	−0.0003
27	37 ± 2	32	o-cresol	0.0063	0.00062	0.0070	−0.0001	−0.0007

Notes: [1] Experiments conducted at a wavelength = 300 nm; [2] The average and standard deviation for triplicate samples. Expt # = Experiment number.

2.4. Experimental Methods

2.4.1. Degradation Experiments

Photocatalytic reactions were performed using a modified Rayonet RPR–100 UV photocatalytic chamber (The Southern New England Ultraviolet Company, Branford, CT, USA) (Figure 1). In order to regulate and monitor the temperature, the photocatalytic chamber was placed in an environmental chamber set at 37 °C (MaxQ 5000, Barnstead, IA, USA). The photochemical reactor was constructed with 16 monochromatic phosphor-coated UV lamps on an outer perimeter (The Southern New England Ultraviolet Company, Branford, CT, USA). The lamps are capable of radiating 300-nm UV light. The irradiance (9 mW cm^{-2}) was measured using a UVX Radiometer (UV Process Supply, Chicago, IL, USA). Prior to initiating the experiments, the lamps were turned-on for at least 1 hour to ensure that full intensity was achieved.

The reaction vessels (25 mm ID × 250 mm) were constructed from Pyrex® and fused quartz tubing (UV transmittant clear fused quartz (GE 214, Technical Glass Products Inc., Painesville Twp., OH, USA)). The Pyrex® upper portion of the vessel was connected to the fused quartz bottom using a graded seal (Technical Glass Products, Inc., Painesville Twp., OH, USA). The reaction tubes were wrapped in Aluminum foil before placing them in the reaction chamber, so as to prevent the initiation of the reaction from extraneous light sources. The tubes were placed on a 5-rpm carrousel in the reaction chamber.

Figure 1. Experimental apparatus.

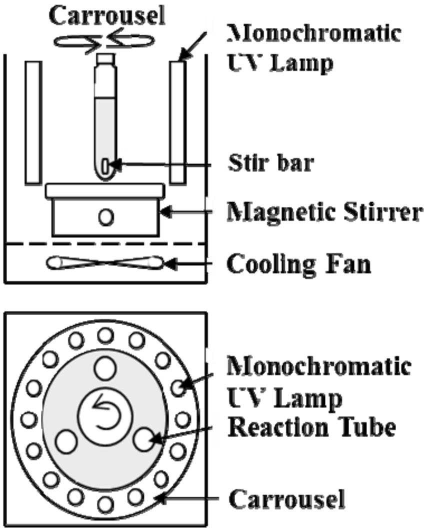

The 50-mL reaction mixture consisted of TiO_2 slurry (1 mg mL^{-1} TiO_2) and reactant (100 mg L^{-1}). All the solutions were prepared with Milli-Q® grade water. The TiO_2 concentration selected was based on work by Gogate and Pandit [16]. The reactant level (100 mg L^{-1}) was based on work from previous studies (Ray *et al.* [37]). Studies by Ray *et al.* [37] have concluded that the phenol degradation rate was optimum at concentrations ranging from 50 to 100 mg L^{-1} with a catalyst concentration of 1 mg mL^{-1}. The mixture was purged for 2 minutes with oxygen (BOC, Windsor, ON, Canada). After purging, the tubes were sealed immediately with Teflon® septa and an Aluminum crimp cap (Cobert Associates, St. Louis, MO, USA). Next, the tubes were conditioned to the desired experimental temperature (30 °C or 37 °C) in an incubator (Blue M Electric Company, White Deer, PA, USA) for 10 minutes.

Immediately after initiating the reaction, a 1-mL sample was removed by inverting the reaction vessel. The sample was placed in an Aluminum foil wrapped vial and stored at 4 °C. In order to maintain a constant reaction volume and catalyst concentration, 1 mL of the 1 mg mL^{-1} TiO_2 slurry was injected into the reaction vessel. The reaction was initiated by removing the Aluminum foil wrap and placing the tubes onto a rotating carrousel in the vessel, which housed the reaction tubes. The contents of the tubes were mixed using magnetic stirrers. Samples were removed at 5-minute intervals. The sample tubes were centrifuged (IEC Centra-8, International Equipment Company, Nashville, TN, USA) at 4000 rpm for 8 minutes to separate the TiO_2 particles from the aqueous solution. After centrifugation, the clear centrate was removed and injected into 2-mL amber vials and stored at 4 °C. All experiments were conducted in triplicate. Controls were prepared under the following conditions: TiO_2/no UV (dark), no TiO_2/UV (photolysis control) and no TiO_2/no UV (normalized control). Controls were prepared to assess the changes in the reactant concentration due to the addition of the TiO_2 slurry (1 mg mL^{-1} TiO_2) and UV.

2.4.2. Surface Area Measurements

The TiO_2 nanoparticle surface area (m^2 g^{-1}) was determined using a Brunauer–Emmett–Teller (BET) gas adsorption technique in a Quantachrome NOVA 1200e surface area analyzer (Quantachrome

Instruments, Boynton Beach, FL, USA). The instrument temperature was set at 77 K, and nitrogen (BOC, Windsor, ON, Canada) was the adsorbate. The relative pressure (P/P_o) range was 0.0 to 0.3.

2.5. Analytical Methods

Samples were analyzed using a Dionex UltiMate 3000 high-performance liquid chromatograph (HPLC) configured with an UltiMate photodiode array detector (PDA) (Dionex, Sunnyville, CA, USA) and a Dionex Acclaim™ 120 C18 3 µm 120Å 2.1 × 100 mm analytical column (Dionex, Sunnyville, CA, USA). The oven temperature was set at 45 °C. The phenol analysis was isocratic and was conducted using an eluent consisting of acetonitrile (20%) (HPLC grade, Burdick & Jackson, Muskegon, MI, USA) plus Milli–Q® water (80%). The flow rate was set at 0.4 mL min^{-1} with a sample injection volume of 25 µL. The analysis was conducted at 191, 210, 226 and 274 nm. The detection limit for phenol was 5 µg L^{-1}. The analysis of o-cresol and m-cresol was conducted under isocratic conditions using an acetonitrile (40%) plus Milli-Q® water (60%) mixture. The flow rate was set at 0.4 mL min^{-1} with a sample injection volume of 25 µL. The analysis was conducted at 210, 226 and 273 nm. The detection limits for m- and o-cresol were 8 µg L^{-1} and 5 µg L^{-1}, respectively. All degradation experiments were conducted at an initial pH of 7 [38]. The pH of the reactor solution was adjusted to pH 7 before the reaction using 1 M HCl and 1 M NaOH. The pH was not adjusted during the reaction. The pH was determined using a pH meter (Symphony, VWR, Mississauga, ON, Canada).

2.6. Optimization Study

A response surface optimization study was conducted using the data from Table 3. In this study, the response variable is the apparent degradation rate constant (k). A modified second-order model (Equation (1)) proposed by Draper and John [34] was used to correlate the experimental variables (reactant type (z), temperature (x_1) and TiO_2 particle size (x_2)) with the response, k′.

$$Y = \beta_o + \sum_{i=1} \beta_i x_i + \sum_{i=1} \beta_{ii} {x_i}^2 + \sum_{i \leq j} \beta_{ij} x_i x_j + \sum_{i=1} \gamma_i z_i + \sum_{i} \sum_{j} \delta_{ij} x_i z_j + \epsilon \tag{1}$$

Y is the predicted response; β_o is a constant; β_I is the linear coefficient; β_{ii} is the squared coefficient; β_{ij} is the cross-product coefficient; and i and j are the index numbers for pattern, $x_1, x_2, \ldots, x_k$. The quantitative factors are designated by x. γ_i is a constant due to the qualitative factor, z_i, and δ_{ij} is the coefficient for the $x_i z_j$ term. ε is the random error.

For 2 quantitative and 1 qualitative factor, Equation (1) becomes:

$$Y_1 = \beta_o + \beta_1 x_1 + \beta_2 x_2 + \beta_{11} {x_1}^2 + \beta_{22} {x_2}^2 + \beta_{12} x_1 x_2 + \gamma z + \gamma_1 x_1 z + \gamma_2 x_2 z \tag{2}$$

Polymath 6.2 (Willimantic, CT, USA) was used to analyze the data and to develop the model. An analysis of variance (ANOVA) was performed to evaluate the model. The D-optimality index was used to establish optimum conditions for maximizing the degradation rate constant [26]. Validating of the model was conducted by correlating the predicted and experimental degradation rate constants and using the Anderson–Darling (AD) statistic [39].

3. Results and Discussion

3.1. Photolytic and Photocatalytic Degradation

A comparison of the different light and dark conditions (TiO_2/no UV (dark control), no TiO_2/UV (photolysis) and TiO_2/UV (photocatalysis)) was used to demonstrate the importance of irradiating the aqueous system containing the TiO_2 catalyst and reactant with UV light. Phenol degradation was examined under all of the conditions ((TiO_2/no UV (dark control), no TiO_2/UV (photolysis) and TiO_2/UV (photocatalysis)) (Tables 3 and 4, Figure 2). The residual concentration profile indicated very little catalytic activity in controls with TiO_2 and no exposure to UV. In the presence of UV plus the TiO_2 catalyst, the increase in phenol degradation was greater when compared to the system containing only the TiO_2 catalyst. The trend observed for phenol under the different reaction conditions shown in Figure 2 was similar to the data for m-cresol and o-cresol [40]. The dependence of the photolytic reaction as a function of temperature for the different reactants is shown in Table 4.

Table 4. Photolytic apparent degradation rate constants for phenol, m-cresol and o-cresol.

Reactant	**Temperature (°C)**	**Apparent degradation rate constant (min^{-1})**	
		Photolysis [1]	
		Average	**SD** [2]
Phenol	23	0.0029	0.0001
Phenol	30	0.0037	0.0003
Phenol	37	0.0037	0.0003
m-Cresol	23	0.0039	0.0002
m-Cresol	30	0.0043	0.0002
m-Cresol	37	0.0056	0.0004
o-Cresol	23	0.0034	0.0001
o-Cresol	30	0.0037	0.0001
o-Cresol	37	0.0050	0.0006

Note: [1] Average and standard deviation for triplicate samples; [2] SD = standard deviation.

Dark controls were used to assess the significance of UV light and TiO_2 on the degradation of a reactant. In the absence of light, the photocatalyst should remain inactive, since there were no photo-generated electrons to mediate the degradation of the reactant. Therefore, any observed degradation would be attributed to the adsorption onto the catalyst. Dark controls were prepared for all experimental conditions and in all of the conditions examined, the reactant profiles were similar.

The reactant concentration for the dark controls was reduced by approximately 3% over a one-hour sampling period. Hence, phenol removal due to adsorption with subsequent degradation was minimal and did not contribute significantly to the photocatalytic process. A careful examination of the data in Tables 3 and 4 strongly suggests that photocatalysis, as well as photolysis mediated the degradation of the reactants when TiO_2 was activated by UV.

Figure 2. A comparison of the residual concentration profiles for phenol under the following conditions: (**a**) 5-nm TiO_2 particles; (**b**) 10-nm TiO_2 particles; and (**c**) 32-nm TiO_2 particles. Temperature = 30 °C, and wavelength = 300 nm. Values are the average and SD for triplicate samples.

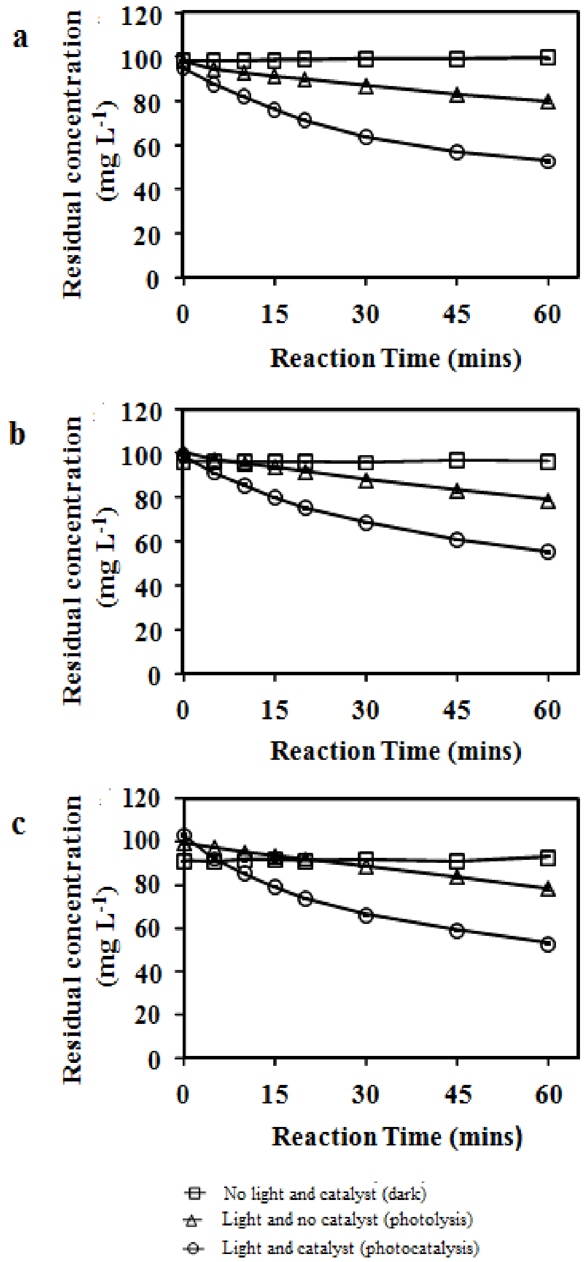

The degradation process was modeled using an integrated first-order expression (Equation (3)).

$$-\frac{dC}{dt} = k_1 c \tag{3}$$

The rate constant, k_1 (min^{-1}), hereafter referred to as the apparent degradation rate constant, is considered as the response. The integrated first-order kinetic expression (Equation (4)) ((–) ln (C/C_o) *versus* time (mins) is plotted for the following conditions: (1) the absence of TiO_2 and the presence of UV (photolysis); and (2) the presence of TiO_2 plus UV (photocatalysis) for the three reactants (Figure 3).

$$\ln\frac{C}{C_o} = -k_1 t \qquad (4)$$

The experimental apparent degradation rate constant was determined from the slope of Equation (3). Least-squares regression values (r^2) of the degradation rate constant data for phenol, m-cresol and o-cresol photolysis ($r^2 > 0.9747$) and photocatalysis ($r^2 > 0.9372$) suggest a reasonably good fit between ln (C/C_o) and time. Though the residual reactants concentrations were used to evaluate the degradation process, it should be noted that total organic carbon (TOC) removal measurements are also suitable.

Figure 3. First-order kinetic plots for photolytic and photocatalytic studies using 300 nm. The experimental conditions were as follows: (**a**) phenol, 5-nm TiO_2 and 37 °C; (**b**) m-cresol, 5-nm TiO_2 and 37 °C; and (**c**) o-cresol, 5-nm TiO_2 and 30 °C (see Table 3). Values are the average and SD for triplicate.

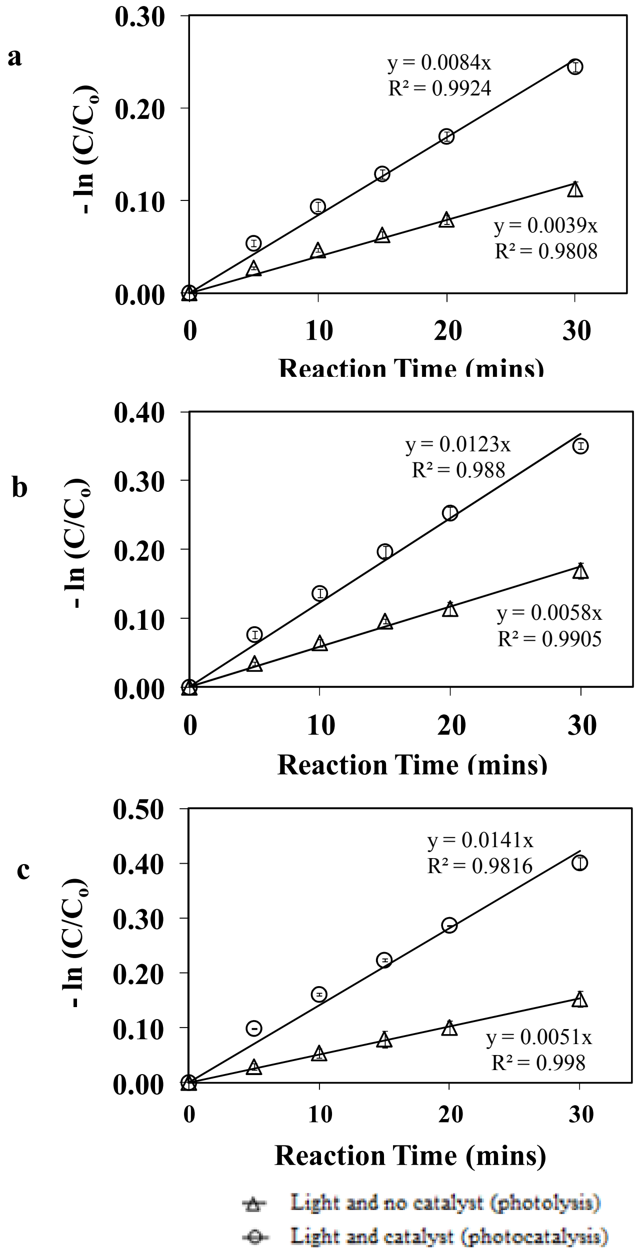

An example plot for phenol degradation using different catalyst particle sizes is shown in Figure 3. The 27 conditions examined and the response variable are shown in Table 3. In the presence of the 5 nm- and 10 nm-sized TiO_2 catalyst, a substantial increase in the apparent degradation rate constant clearly indicate the addition of a catalyst coupled with UV increased the degradation of phenol, m-cresol and o-cresol. The apparent degradation rate constants for reactions conducted with 32-nm TiO_2 particles showed a relatively small increase in the photocatalytic activity when compared to photolysis.

3.2. Effect of the Variables on the apparent degradation constant

The impact of various reaction variables on the UV/TiO_2 photocatalytic degradation of substrates, such as di-(2-ethylhexyl) phthalate (DEHP) and dibutyl phthalate (DPB), has been extensively reported in several studies using a one-factor-at-a-time approach [41–43]. Employing a one-factor-at-a-time approach is problematic because the interaction between different factors could also affect the response variable. In the present work, the effect of three experimental factors on the apparent degradation rate constant was examined. A rise in the apparent degradation rate constant with increasing temperature was observed for phenol, m-cresol and o-cresol at each particle size (5, 10 and 32 nm) (Figure 4). The increase in the degradation rate constant was most likely due to the enhanced collision frequency with increasing reaction temperature [41].

Figure 4. Main effect plots for the experimental factors.

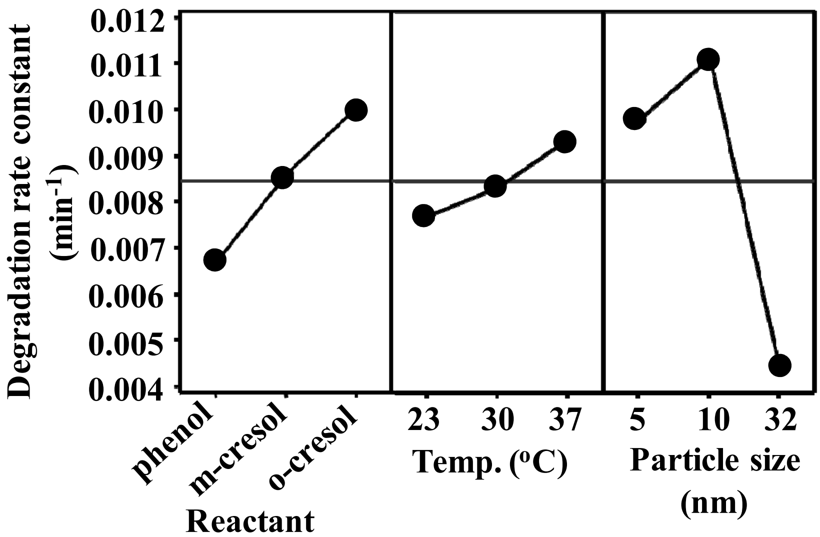

Note for the three particle sizes under consideration, the average value for the change in the rate constant (min^{-1}) per °C rise for phenol, m-cresol and o-cresol was 0.00005–0.0001, 0.0008–0.0002 and 0.0005–0.0003, respectively. The largest change in the rate constant (min^{-1}) per °C was associated with o-cresol. Increasing the temperature by 14 °C caused the phenol degradation rate constant to increase by approximately 60% for the 5-nm particles; however, no significant increase was observed for the substituted phenols. An optimum apparent degradation rate constant was observed for 10-nm particles with phenol, m-cresol and o-cresol (Figure 4). This trend is in agreement with studies which have examined the relationship between particle size and photocatalytic reactivity. Increasing the photocatalytic activity with decreasing particle size for TiO_2 nanoparticles containing anatase and rutile in various proportions was demonstrated in studies by Almquist and Biswas [44]. This trend could be attributed to the off-setting contributions of a high surface area, as well as changes in the structural and electronic properties of the TiO_2 as the particle size decreases in the nanometer scale [43]. Similar work with anatase concluded that 11-nm TiO_2 particles yielded the highest photonic efficiency [45]. According to Zhang *et al.* [46], TiO_2 nanoparticles less than 10 -nm have a tendency to form stable agglomerates in aqueous solution. These agglomerates are classified as primary and secondary particles and denoted as non-aggregated and aggregated particles, respectively. Studies by Zhang *et al.* [46] and Lin *et al.* [47] have shown that the degradation rates for primary particles are greater than those for secondary particles. Lower surface areas are associated with aggregates when compared to the individual particles and hence, lower reaction rates are expected with increasing the size of the agglomerates. In this study, similar or lower reaction rates for the 5-nm TiO_2 nanoparticles in comparison to the 10-nm nanoparticles was likely associated with the formation of aggregates [46]. The data clearly indicate that an increase in the apparent degradation rate constant resulted in greater photocatalytic efficiency. The optimum apparent degradation rate constant observed with 10-nm particles is similar to work reported by Ray *et al.* [27] for phenol degradation by 9-nm nanoparticles. The selectivity of the TiO_2 catalyst for the different substrates is reflected by the change in the apparent degradation rate constant with the substrate chemical structure. Increasing the apparent degradation rate constant for the different substrates was as follows: o-cresol > m-cresol > phenol, for each particle size (Figure 4). The differences in the apparent degradation rate constant between phenol and the cresol isomers could be explained by examining the intermediates formed during the degradation pathway. The degradation mechanism is dependent on the position of the substituted methyl group relative to the OH group on the benzene ring. The addition of •OH radicals in the photocatalytic oxidation process proceed by an electrophilic addition reaction [48]. According to Bhatkhande *et al.* [20], different intermediates are produced depending on the position of the substituted group with respect to the OH position on the benzene ring. During the hydroxylation of cresols, the ortho site between the OH and methyl functional groups in m-cresol are susceptible to attack by •OH radicals. Hence, only three sites are available to react with the •OH radical [17]. A reduction in the number of available sites for •OH attack in the m-cresol structure when compared to o-cresol could be a possible cause for the lower apparent degradation rate constant.

3.3. Combined Effects of the Experimental Variables

The apparent degradation rate constants for all of the photocatalytic experiments (Table 3) were statistically analyzed to assess the effects of the experimental variables on the apparent degradation rate constant. The ANOVA analysis (Table 5) indicates that the factors under consideration on the apparent degradation rate constant are significant at a 95% level of confidence. The *p*-values for particle size, temperature and reactant suggest that they were significant. An interaction was observed only for a paired combination of particle sizes. No mixed interaction terms were significant within the factor space evaluated because the *p*-values for the terms were >0.05 at a 95% level of confidence.

Table 5. ANOVA results for the experimental response at different factor levels.

Source	DF	Seq SS	Adj SS	Adj MS	F	*p*	
Regression	8	0.000289	0.000289	0.000036	82.10	0.000	S
Linear							
x_1	1	0.000012	0.000012	0.000012	28.42	0.000	S
x_2	1	0.000127	0.000127	0.000127	289.81	0.000	S
z	1	0.000050	0.000050	0.000050	114.44	0.000	S
Square							
$x_1 \times x_1$	1	0.000000	0.000000	0.000000	0.49	0.494	NS
$x_2 \times x_2$	1	0.000096	0.000096	0.000096	217.66	0.000	S
Interaction							
$x_1 \times x_2$	1	0.000000	0.000000	0.000000	0.68	0.419	NS
$x_1 \times z$	1	0.000000	0.000000	0.000000	1.09	0.310	NS
$x_2 \times z$	1	0.000002	0.000002	0.000002	4.19	0.056	NS
Residual Error	18	0.000008	0.000008	0.000000			
Total	26	0.000297					

Notes: R^2 = 97.33%, R^2 (predicted = 93.62%, R^2 (adjusted) = 96.15%; S = significant; NS = Not significant; DF = Degrees of freedom; Seq SS = Sequential sum of squares; Adj SS = Adjusted sum of squares; Adj MS = Adjusted mean square; * = multiplication sign.

Contour plots were generated to determine the relationship between the factors. The optimum conditions that resulted in the maximum photoactivity conditions for effective degradation are shown in the contour plots. The contour plots were developed using Equation (6). The contour lines represent values of the apparent degradation rate constant in terms of a combination of factors including temperature *versus* reactant (Figure 5a), particle size *versus* reactant (Figure 5b) and particle size *versus* temperature (Figure 5c). An increase in response is observed with increasing coded values for temperature and reactant (Figure 5a). A maximum apparent degradation rate constant value is indicated on each contour plot at the optimum condition for each factor (temperature, particle size and reactant). The particle size *versus* temperature contour plot (Figure 5c) indicates the highest rate at 37 °C and a particle of approximately 10 nm for the three reactants (phenol, m-cresol and o-cresol). The contour plot for particle size *versus* reactant (Figure 5b) demonstrates the impact of the structural properties of the reactant on the degradation rate constant. Under the different temperature conditions (23, 30 and 37 °C), the degradation rate trend for the different reactants was as follows: o-cresol > m-cresol > phenol. The effectiveness of the different factors on influencing the degradation rate constant was the particle size followed by the reactant structure and then temperature (Figure 4). The two-factor interaction plot (Figure 6) suggests no significant interaction between the different factors. Note that the intersecting profiles indicate factor interaction, while parallel profiles are an indicator that the factors are independent.

Figure 5. Contour plots of the apparent degradation rate constant for (**a**) temperature *versus* reactant; (**b**) particle size *versus* reactant; and (**c**) particle size *versus* temperature.

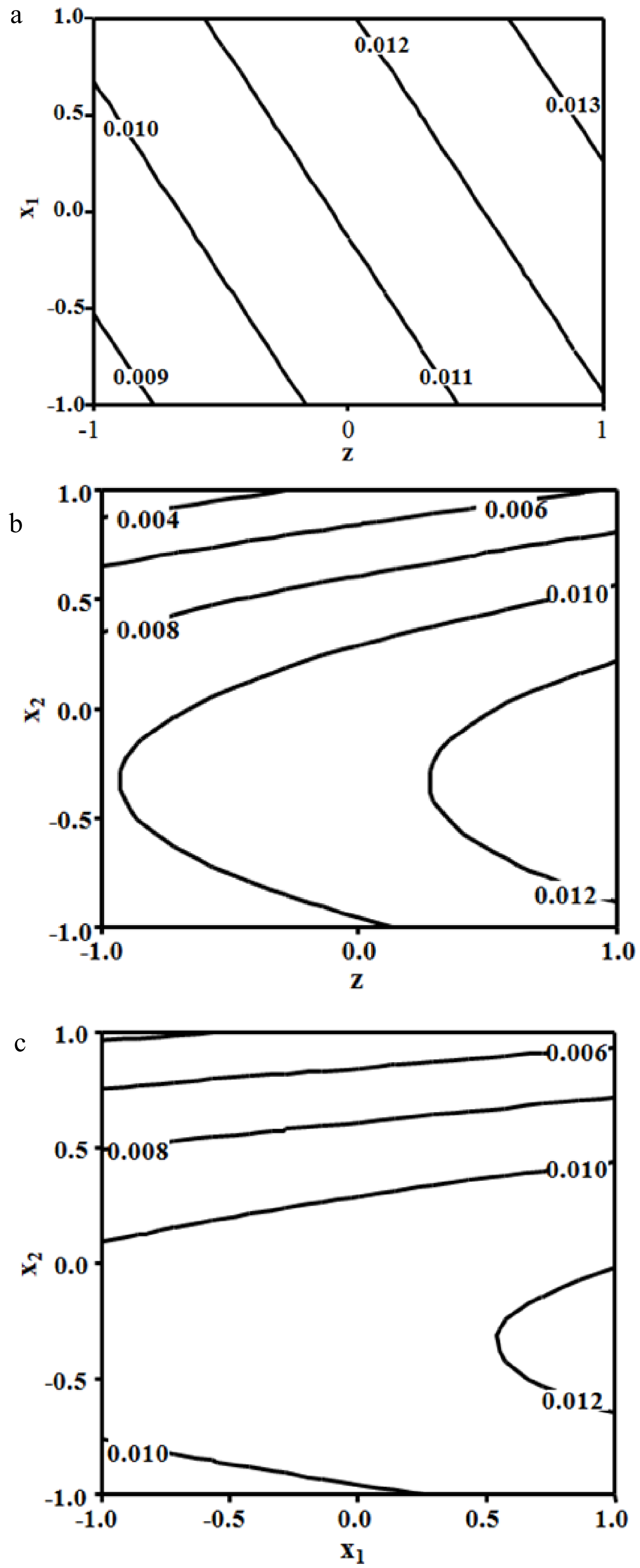

Figure 6. Interaction plots for experimental response data.

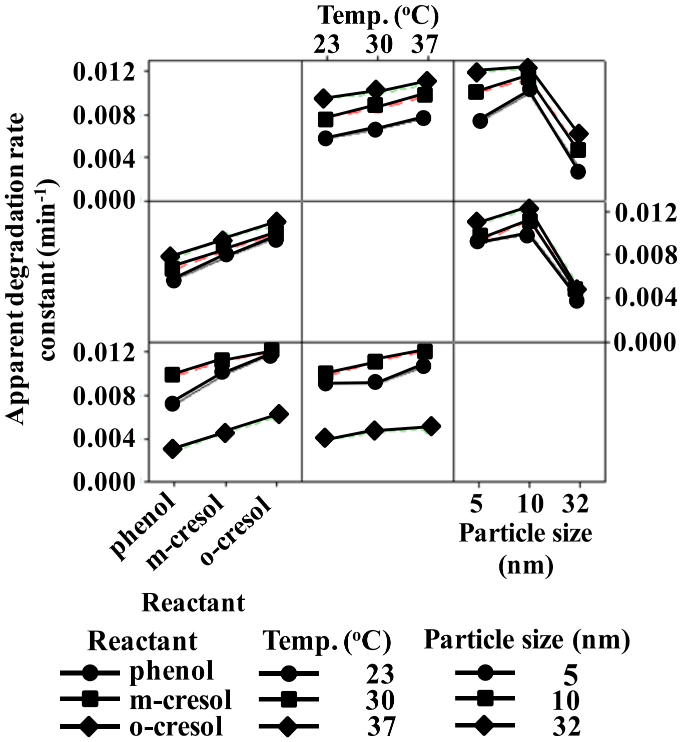

3.4. Model Development

A quadratic polynomial was developed to relate the coded factors and the response using Polymath. Minitab was used to model the data based on the selected second-order (quadratic) model. The regression analysis was conducted using coded units (Table 2). The ANOVA data is shown in Table 5. The regression model (Equation (5)) explained 97.33% of the variation in the degradation rate constant values. The predicted R^2 of 0.9362 is in reasonable agreement with the adjusted R^2 of 0.9615. The model is predictive, since the calculated F-value (82.1) is greater than the critical F-value (3.4). This shows that the model equation is reliable within the range of factors under consideration. This model (Equation (5)) contains insignificant and significant terms in the quadratic equation. The modified model equation (Equation (6)) was developed by neglecting the insignificant terms in the quadratic equation (Equation (5)) (Table 3). The predicted values based on the modified model are depicted in Table 5. The predicted values obtained from the two equations (Equations (5) and (6)) are shown in Figure 7. The comparison indicated no significant difference between the predicted response values for the two models (Figure 7).

$$\begin{aligned} k = 0.10985 + 0.00833\, x_1 - 0.00266\, x_2 + 0.00189\, x_1^2 - 0.003994\, x_2^2 \\ -0.000158\, x_1 x_2 + 0.001672\, z - 0.000200\, z\, x_1 + 0.000392\, z\, x_2 \end{aligned} \tag{5}$$

$$k' = 0.01111 + 0.00833\, x_1 - 0.00266\, x_2 - 0.00399\, x_2^2 + 0.01672\, z \tag{6}$$

In this study, the D-optimal criterion was employed to determine the maximum degradation rate. The D-optimal criterion selects design points from a list of candidate points, such that the variances of the model regression coefficients are minimized. MINITAB (Minitab inc., State College, PA, USA), a statistical software program, was used to generate the optimal value.

Figure 7. Predicted *versus* experimental degradation rate constants. (**a**) Based on Equation (5); (**b**) Based on Equation (6).

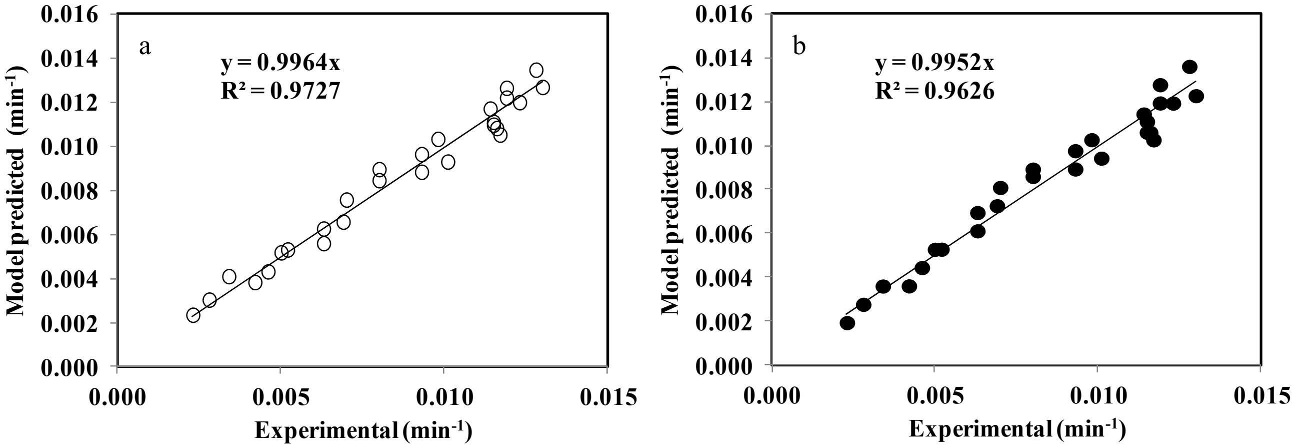

The D-optimality index varies between zero (worst case) and one (ideal case) for all of the factors. The software searches for all possible factor settings and computes a value for the largest D-optimality value. A D-optimality of approximately 0.98 with a maximum response value of 0.0141 min^{-1} was recorded for o-cresol at 37 °C and a TiO_2 particle size of 11 nm (Figure 8). In comparison, for the experiment conducted with o-cresol at 37 °C and a 10-nm particle size catalyst, the response was 0.0128 min^{-1} with a standard deviation of 0.005 min^{-1}. The experimental response was approximately 9.2% less than the predicted maximum response of 0.0141 min^{-1}.

Figure 8. D-Optimality plot.

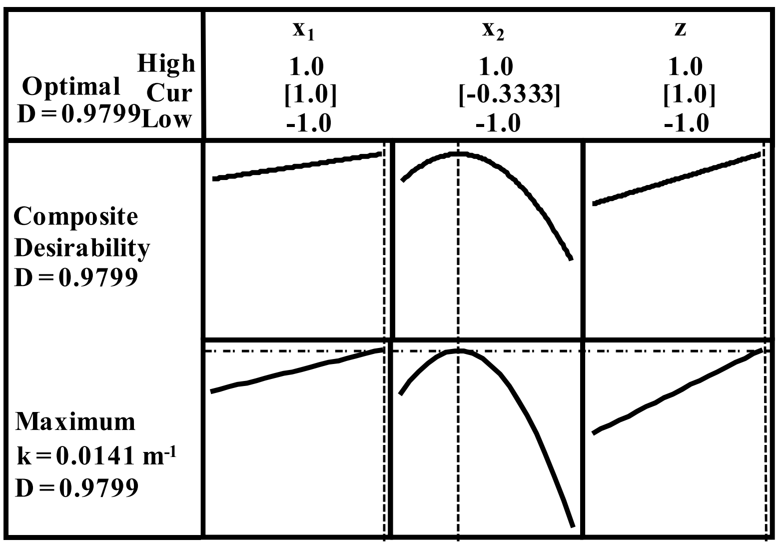

3.5. Assessment of the Model

A plot of the experimental rate constant values *versus* the model predicted values provided an indication of the goodness of fit (Figure 7). An R^2 value of 0.9626 for the modified model (Equation (6)) indicates a reasonable fit. The Anderson–Darling (AD) test was also used to determine the adequacy of the model. The AD statistic for Equation (6) (Figure 9) confirmed a normal-fit for the probability distribution of the residuals. The calculated AD statistic (0.139) was less than the critical value of 0.799 for a sample size of 27 and the associated *p*-value (0.971) of the AD statistic was significant at a 5% level (greater than 0.05) [49]. A lower value of the computed AD statistic compared to the critical value confirmed a normal-fit for the probability distribution of residuals. From this analysis, it appears that the response surface regression model is able to predict the photocatalytic degradation of phenol, m-cresol and o-cresol within the temperature range for TiO_2 catalysts diameter ranging from 5 to 32 nm.

Figure 9. Anderson–Darling (AD) normality plot of the residuals.

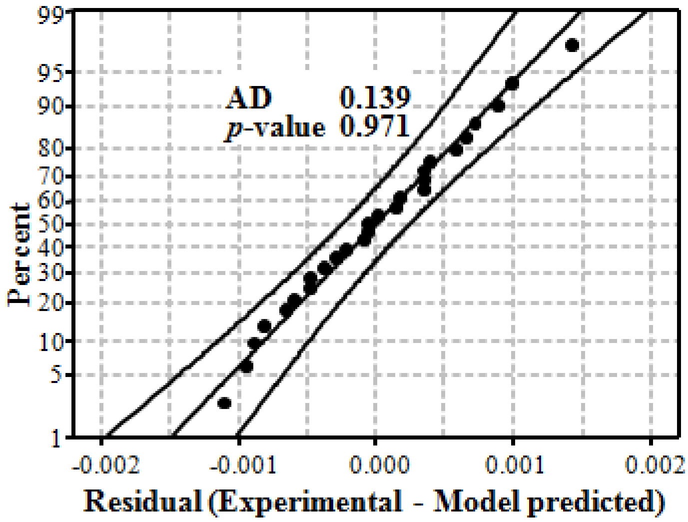

3.6. Activation Energy

A catalyst functions by increasing the reaction rate and lowering the activation energy. Studies by Pande *et al.* [50] have shown that 15-nm Cu_2O nanoparticles are able to reduce the activation energy by approximately 71 kJ mol^{-1} and hence, increase the reaction rate by 2.4×10^7-fold. The reaction rate constant, k_{app}, can be derived from the Arrhenius equation (Equation (7)).

$$\ln k_{app} = \ln A - \frac{E_a}{RT} \tag{7}$$

where k_{app} is the rate constant; A is a constant; E_a is the activation energy; R is the universal gas constant and T is temperature (K). The activation energy (E_a) was obtained from a plot of ln k_{app} *versus* 1/T. The activation energy data tabulated in Table 6 show activation energies as a function of particle size and substrate. No significant correlation between the activation energies and catalyst particle sizes was observed for the three reactants. Evidence by Musselwhite *et al.* [51] has shown that the activation energies for cyclohexenone hydrogenation by 2.9–7.1 nm colloidal platinum nanocatalysts were similar irrespective of the catalyst particle size. However, studies by other researchers have reported conflicting data. Shah *et al.* [52] claim that decreasing catalyst particle sizes correlated with decreasing activating energies, while studies by Patil *et al.* [53] show a proportional increase in activation energy with increasing particle size for the degradation of Congo red dye.

Photocatalytic activation energies typically range from 5 to 15 kJ mol^{-1} in aqueous solutions [54]. The activation energies reported for the catalytic degradation of selected chemicals with the Degussa P25 catalyst range from 13.6 to 24.8 kJ mol^{-1} (Table 7). In this study, the activation energies for o-cresol, m-cresol and phenol (7.0 to 17.1 kJ mol^{-1}) are comparable to those from previous studies. For m-cresol, a statistical analysis using Tukey's method revealed a significant difference between the activation energy for the 5-nm particle in comparison to those for the 10-nm and 32-nm particles (activation energies labeled with superscripts a and b) (Table 6). When comparing the activation energies for different particle sizes, no significant statistical difference was observed for phenol and o-cresol. A significant statistical difference between the activation energies for o-cresol *versus* m-cresol and phenol was observed for 5-nm and 10-nm particle size catalysts. For the 32-nm particle size catalyst, the activation energies (superscript c) were statistically the same for phenol, m-cresol and p-cresol.

Table 6. Activation energies for o-cresol, m-cresol and phenol for different TiO_2 particle sizes.

Particle size (nm)	**o-cresol**	**m-cresol**	**phenol**
	Activation energy (kJ mol^{-1})		
5	$6.97 \pm 5.88^{a,c}$	$17.12 \pm 1.18^{a,d}$	$10.62 \pm 2.01^{a,d}$
10	$3.13 \pm 1.61^{a,c}$	$13.02 \pm 1.18^{b,d}$	$12.52 \pm 2.76^{a,d}$
32	$10.45 \pm 4.81^{a,c}$	$11.63 \pm 1.57^{b,c}$	$15.78 \pm 1.56^{a,c}$

Notes: All values are averages for triplicate samples; data set pairs labeled using dissimilar letters (a, b) within the same columns are statistically different at a 95% confidence interval using Tukey's procedure [49]; data set pairs labeled using dissimilar numbers (c, d) within the same rows are statistically different at a 95% confidence interval using Tukey's procedure [49].

Table 7. Activation energies for selected reactants using Degussa P25 catalyst.

TiO_2 catalyst	**Reactant**	**Temperature (K)**	**Activation Energy (kJ mol^{-1})**	**Reference**
Degussa P25	Phenol	303–329	16.2	Kartal *et al.*[55]
Degussa P25	Naphthalene	283–313	22.0	Lair *et al.* [56]
Degussa P25	Imazaquin	293–313	24.8	Garcia *et al.*[57]
Degussa P25	Phenol	290–303	13.6	Ray *et al.*[27]
Degussa P25	Phenol	296–310	10.6–15.8	This study
Degussa P25	o-Cresol	296–310	7.0–10.5	This study
Degussa P25	m-Cresol	296–310	11.6–17.1	This study

4. Conclusions

The novel modeling technique used and described in this study can be used in similar studies involving the use of both quantitative and qualitative factors. The study indicated that effluents containing phenol, o-cresol and m-cresol mixtures within the levels under consideration were treatable using TiO_2 photocatalysis. The optimum values of experimental factors were determined for the maximum degradation of the three compounds. The optimum values of the factors indicated can be adopted for further laboratory experiments and pilot-scale organic pollutants removal processes.

The conclusions from this study are as follows:

1. Ten nanometer diameter TiO_2 particles combined with an operating temperature of 37 °C were the optimum conditions to effectively degrade the reactants.
2. The apparent degradation rate constant trend for the reactants was as follows: o-cresol > m-cresol > phenol.

3. No interaction effects were observed between the experimental factors (particle size, temperature and reactant). The interaction was observed only for a paired combination of particle sizes.
4. The modified response surface regression model was adequate for relating the apparent degradation rate constant to the experimental factors within the range of conditions under consideration.
5. The apparent degradation rate constant followed an Arrhenius temperature dependence with an increasing linear trend for the three reactants.
6. The activation energy was lowest for the degradation of o-cresol using 10-nm TiO_2 particles.

Similar studies with immobilized TiO_2 nanoparticles are recommended for future work and pilot-scale studies are required before commercial application.

Acknowledgments

Financial support for this work was provided by Consulting Engineers of Ontario, the Natural Sciences and Engineering Research of Canada (NSERC) and the Canada Research Chair program and the University of Windsor. Srimanta Ray assisted with the experimental design and surface area measurements.

Author Contributions

The experimental work was conducted by Marissa Choquette-Labbé. The manuscript was written by Wudneh A. Shewa and Jerald A. Lalman. Data analysis and the model development were performed by Jerald A. Lalman, Wudneh A. Shewa and Saravanan R. Shanmugam.

Conflicts of Interest

The authors declare no conflict of interest.

References

1. World Health Organization. *Phenol: Environmental Health Criteria 161*; World Health Organization: Geneva, Switzerland, 1994.
2. World Health Organization. *Cresols: Environmental Health Criteria 168*; World Health Organization: Geneva, Switzerland, 1995.
3. European Union. The list of priority substances in the field of water policy and amending directive, Council directive 2455/2001/ECC. Official Journal of the European Communities L331, 20 November 2001, pp 1–5.
4. Environment Canada. *The Second Priority Substances List (PSL2) of the Canadian Environmental Protection Act (CEPA)*; Environment Canada: Gatineau, Canada, 1995.
5. United States Environmental Protection Agency (USEPA). *Sampling and Analysis Procedure for Screening of Industrial Effluents for Priority Pollutants*; Environment Monitoring and Support Laboratory: Cincinnati, OH, USA, 1977.

6. Pfeffer, F.M. The 1977 screening survey for measurement of organic priority pollutants in petroleum refinery wastewaters. *ASTM Specif. Tech. Publ.* **1979**, *686*, 181–190.
7. Keith, L.H. Identification of organic compounds in unbleached treated kraft paper mill wastewaters. *Environ. Sci. Technol.* **1976**, *10*, 555–564.
8. Parkhurst, B.R.; Bradshaw, A.S.; Forte, J.L. An evaluation of the acute toxicity to aquatic biota of a coal conversion effluent and it major components. *Bull. Environ. Contam. Toxicol.* **1979**, *23*, 349–356.
9. Jungclaus, G.; Avila, V.; Hites, R. Organic compounds in an industrial wastewater: A case study of their environmental impact. *Environ. Sci. Technol.* **1978**, *12*, 88–96.
10. Kamenev, I.; Munter, R.; Pikkov, L.; Kekisheva, L. Wastewater treatment in oil shale chemical industry. *Oil Shale* **2003**, *20*, 443–457.
11. Guo, Z.; Ma, R.; Li, G. Degradation of phenol by nanomaterial TiO_2 in wastewater. *Chem. Eng. J.* **2006**, *119*, 55–59.
12. Auriol, M.; Filali-Meknassi, Y.; Tyagi, R.D.; Adams, C.D.; Surampalli, R.Y. Endocrine disrupting compounds removal from wastewater, a new challenge. *Process Biochem.* **2006**, *41*, 525–539.
13. Cooper, V.A.; Nicell, J.A. Removal of phenols from a foundry wastewater using horseradish peroxidise. *Water Res.* **1996**, *30*, 954–964.
14. Veeresh, G.S.; Kumar, P.; Mehrotra, I. Treatment of phenol and cresols in upflow anaerobic sludge blanket (UASB) process: A review. *Water Res.* **2005**, *39*, 154–170.
15. Hobson, M.J.; Millis, N.F. Chemostat studies of a mixed culture growing on phenolics. *Res. J. Water Poll. Control Fed.* **1990**, *62*, 684–691.
16. Gogate, P.R.; Pandit, A.B. A review of imperative technologies for wastewater treatment I: Oxidation technologies at ambient conditions. *Adv. Environ. Res.* **2004**, *8*, 501–551.
17. Wang, K.H.; Hsieh, Y.H.; Chen, L.J. The heterogeneous photocatalytic degradation, intermediates and mineralization for the aqueous solution of cresols and nitrophenols. *J. Hazard. Mater.* **1998**, *59*, 251–260.
18. Matilainena, A.; Sillanpaa, M. Removal of natural organic matter from drinking water by advanced oxidation processes. *Chemosphere* **2010**, *80*, 351–365.
19. Glaze, W.H.; Kang, J.W.; Chapin, D.H. Chemistry of water treatment processes involving ozone, hydrogen peroxide and ultraviolet radiation. *Ozone Sci. Eng.* **1987**, *9*, 335–352.
20. Bhatkhande, D.S.; Pangarkar, V.G.; Beenackers, A. Photocatalytic degradation for environmental applications—A review. *J. Chem. Technol. Biotechnol.* **2001**, *77*, 102–116.
21. Dalrymple, O.K.; Yeh, D.H.; Trotz, M.A. Review: Removing pharmaceuticals and endocrine-disrupting compounds from wastewater by photocatlysis. *J. Chem. Technol. Biotechnol.* **2007**, *82*, 121–134.
22. Bouzouba, A.; Markovits, A.; Calatayud, M.; Minot, C. Comparison of the reduction of metal oxide surfaces: TiO_2-anatase, TiO_2-rutile and SnO_2-rutile. *Surf. Sci.* **2005**, *583*, 107–117.
23. Hengerer, R.; Bolliger, B.; Erbudak, M.; Grätzel, M. Structure and stability of the anatase TiO_2 (101) and (001) surfaces. *Surf. Sci*. **2000**, *460*, 162–169.
24. Ahmed, S.; Rasul, M.G.; Martens, W.N.; Brown, R.; Hashib, M.A. Advances in heterogeneous photocatalytic degradation of phenols and dyes in wastewater: A review. *Water Air Soil Pollut.* **2011**, *215*, 3–29.

25. Mehrotra, K.; Yablonsky, G.S.; Ray, A.K. Kinetic studies of photocatalytic degradation in a TiO_2 slurry system: Distinguishing working regimes and determining rate dependences. *Ind. Eng. Chem. Res.* **2003**, *42*, 2273–2281.
26. Mehrotra, K. Yablonsky, G.S.; Ray, A.K. Macro kinetic studies for photocatalytic degradation of benzoic acid in immobilized systems. *Chemosphere* **2005**, *60*, 1427–1436.
27. Ray, S.; Lalman, J.A.; Biswas, N. Using the Box-Benkhen technique to statistically model phenol photocatalytic degradation by titanium dioxide nanoparticles. *Chem. Eng. J.* **2009**, *150*, 15–24.
28. Wang, J.; Wan, W. Optimization of fermentative hydrogen production process using genetic algorithm based on neural network and response surface methodology. *Int. J. Hydrog. Energy* **2009**, *34*, 255–261.
29. Yetilmezsoya, K.; Demirel, S.; Vanderbei, R.J. Response surface modeling of Pb (II) removal from aqueous solution by Pistacia vera L.: Box-Behnken experimental design. *J. Hazard. Mater.* **2009**, *171*, 551–562.
30. Myers, R.H.; Montgomery, D.C.; Anderson-Cook, C.M. *Response Surface Methodology: Process and Product Optimization Using Designed Experiments*, 3rd ed.; Wiley & Sons: New York, NY, USA, 2009.
31. Kowalski, S.; Cornell, J.A.; Vining, G.G. A new model and class of designs for mixture experiments with process variables. *Commun. Stat. Theory Methods* **2000**, *29*, 2255–2280.
32. Quinn, G.P.; Keough, M.J. Multiple and complex regression. In *Experimental Design and Data Analysis for Biologists*; Cambridge University Press: London, UK, 2002; pp. 130–139.
33. Daly, L.; Bourke, G.J. Multivariate analysis and the control of cofounding. In *Interpretation and Uses of Medical Statistics*; Blackwell Sciences Ltd.: London, UK, 2000; pp. 340–348.
34. Draper, N.R.; John, J.A. Response-surface designs for quantitative and qualitative factors. *Technometrics* **1988**, *30*, 423–428.
35. Aggarwal, M.L.; Chowdhury, S.R.; Bansa, A.; Mita, N. Efficient response surface designs with quantitative and qualitative factors. *J. Ind. Soc. Agric. Stat.* **2006**, *60*, 90–99.
36. Allen, T.T.; Tseng, S.-H. Variance plus bias optimal response surface designs with qualitative factors applied to stem choice modeling. *Qual. Reliab. Eng. Int*. **2011**, *27*, 1199–1210.
37. Ray, S.; Lalman, J.A.; Biswas, N. Heterogeneous photocatalytic degradation of phenol by titanium dioxide nanoparticles: An optimization approach. In Proceedings of the AIChE Annual Meeting, Salt Lake City, UT, USA, 4–7 November 2007.
38. Aliabadi, M.; Ghahremani, H.; Izadkhah, F.; Sagharigar, T. Photocatalytic degradation of N-methyl-2-pyrrolidone in aqueous solutions using light sources of UVA, UVC and UVLED. *Fresenius Environ. Bull.* **2012**, *21*, 2120–2125.
39. Stephens, M.A. Tests based on EDF statistics. In *Goodness-of-fit Techniques*; D'Agostino, R.B., Stephens, M.A., Eds.; CRC Press: New York, NY, USA, 1986; pp. 97–194.
40. Labbe, M. Photocatalytic degradation of select drinking water pollutants using nano-titanium dioxide catalyst. M.A.Sc Thesis, University of Windsor, Windsor, Ontario, Canada, 2008.
41. Zhu, S.; Yang, X.; Yang, W.; Zhang, L.; Wang, J.; Huo, M. Application of porous nickel-coated TiO_2 for the photocatalytic degradation of aqueous quinoline in an internal airlift loop reactor. *Int. J. Environ. Res. Public Health* **2012**, *9*, 548–563.

42. Chung, Y.C.; Chen, C.Y. Degradation of Di-(2-ethylhexyl) phthalate (DEHP) by TiO_2 photocatalysis. *Water Air Soil Pollut.* **2009**, *200*, 191–198.
43. Kaneco, S.; Katsumata, K.; Suzuki, T.; Ohta, K. Titanium dioxide mediated photocatalytic degradation of dibutyl phthalate in aqueous solution: Kinetics, mineralization and reaction mechanism. *Chem. Eng. J.* **2006**, *125*, 59–66.
44. Almquist, C.B.; Biswas, P. Role of synthesis method and particle size of nanostructured TiO_2 on its photoactivity. *J. Catal.* **2002**, *212*, 145–156.
45. Zhang, Z.; Wang, C.C.; Zakaria, R.; Ying, J.Y. Role of particle size in nanocrystalline TiO_2 based photocatalysts. *J. Phys. Chem. B* **1998**, *102*, 10871–10878.
46. Zhang, Y.; Chen, Y.; Westerhoff, P.; Hristovski, K.; Crittenden, J.C. Stability of commercial metal oxide nanoparticles in water. *Water Res.* **2008**, *42*, 2204–2212.
47. Lin, H.; Huang, C.P.; Li, W.; Ni, C.; Shah, S.I.; Tseng, Y.H. Size dependency of nanocrystalline TiO_2 on its optical property and photocatalytic reactivity exemplified by 2-chlorophenol. *Appl. Catal. B* **2006**, *68*, 1–11.
48. Albarran, G.; Bentley, J.; Schuler, R.H. Substituent effects in the reaction of OH radicals with aromatics: Toluene. *J. Phys. Chem. A* **2003**, *107*, 7770–7774.
49. Stephens, M.A. EDF statistics for goodness of fit and some comparisons. *J. Am. Stat. Assoc.* **1974**, *69*, 730–737.
50. Pande, S.; Jana, S.; Basu, S.; Sinha, A.K.; Datta, A.; Pal, T. Nanoparticle-catalyzed clock reaction. *J. Phys. Chem. C* **2008**, *112*, 3619–3626.
51. Musselwhite, N.E.; Wagner, S.B.; Manbeck, K.A.; Carl, L.M.; Gross, K.M.; Marsh, A.L. Activity and selectivity of colloidal platinum nanocatalysts for aqueous phase cyclohexenone hydrogenation. *Appl. Catal. A* **2011**, *402*, 104–109.
52. Shah, S.I.; Huang, C.P.; Chen, J.G.; Doren, D.; Barteau, M. Semiconductor metal oxide nanoparticles for visible light photocatalysis. In Proceedings of the NSF Nanoscale Science and Engineering Grantees Conference, Arlington, VA, USA, 16–18 December 2003.
53. Patil, S.R.; Akpan, U.G.; Hameed, B.H.; Samdarshi, S.K. A comparative study of the photocatalytic efficiency of Degussa P25, Qualigens, and Hombikat UV-100 in the degradation kinetic of congo red dye. *Desalin. Water Treat.* **2012**, *46*, 188–195.
54. Mills, A.; Davies, R.H.; Worsley, D. Water purification by semiconductor photocatalysis. *Chem. Soc. Rev.* **1993**, *22*, 417–425.
55. Kartal, Ö.E.; Erol, M.; Oğuz, H. Photocatalytic destruction of phenol by TiO_2 powders. *Chem. Eng. Technol.* **2001**, *24*, 645–649.
56. Lair, A.; Ferronato, C.; Chovelon, J.M.; Herrmann, J.M. Naphthalene degradation in water by heterogeneous photocatalysis: An investigation of the influence of inorganic anions. *J. Photochem. Photobiol. A* **2008**, *193*, 193–203.
57. Garcia, J.C.; Takashima, K. Photocatalytic degradation of imazaquin in an aqueous suspension of titanium dioxide. *J. Photochem. Photobiol.* A **2003**, *155*, 215–222.